ISSN 0965-5425, Computational Mathematics and Mathematical Physics, 2017, Vol. 57, No. 6, pp. 1066–1079. © Pleiades Publishing, Ltd., 2017.

Convective Heat and Mass Transfer in Three-Dimensional Mixed Convection Flow of Viscoelastic Fluid in Presence of Chemical Reaction and Heat Source/Sink[1]

M. Bilal Ashraf[b]*, A. Alsaedi[a], T. Hayat[a, c], and S. A. Shehzad[d]

[a] *Nonlinear Analysis and Applied Mathematics (NAAM) Research Group, Department of Mathematics, Faculty of Science, King Abdulaziz University, P. O. Box 80203, Jeddah 21589, Saudi Arabia*

[b] *Department of Mathematics, Comsats Institute of Information Technology, Wah Cantt 47040, Pakistan*

[c] *Department of Mathematics, Quaid-i-Azam University 45320, Islamabad 44000, Pakistan*

[d] *Department of Mathematics, Comsats Institute of Information Technology, Sahiwal 51000, Pakistan*

** e-mail: bilalashraf@ciitwah.edu.pk; ali_qau70@yahoo.com; aalsaedi@hotmail.com*

Received October 22, 2016; in final form, January 9, 2017

Abstract—Heat and mass transfer effects in the three-dimensional mixed convection flow of a viscoelastic fluid with internal heat source/sink and chemical reaction have been investigated in the present work. The flow generation is because of an exponentially stretching surface. Magnetic field normal to the direction of flow is considered. Convective conditions at the surface are also encountered. Appropriate similarity transformations are utilized to reduce the boundary layer partial differential equations into the ordinary differential equations. The homotopy analysis method is used to develop the solution expressions. Impacts of different controlling parameters such as ratio parameter, Hartman number, internal heat source/sink, chemical reaction, mixed convection, concentration buoyancy parameter and Biot numbers on the velocity, temperature and concentration profiles are analyzed. The local Nusselt and Sherwood numbers are sketched and examined.

Keywords: viscoelastic fluid, three dimensional flow, mixed convection flow, exponentially stretching surface, chemical reaction, heat source/sink.

DOI: 10.1134/S0965542517060021

INTRODUCTION

At present the heat and mass transfer over a stretching sheet has gained much importance amongst the researchers due to their engineering applications such as in polymer technology, metallurgy, extrusion process, paper and glass fiber production, manufacturing of plastic and rubber sheets etc. Crane [1] initiated the analysis of boundary layer flow of viscous fluid over a stretching plate with linear velocity. Afterwards such work is analyzed through different aspects including suction/injection, MHD, internal heat generation/absorption, power law heat flux, mixed convection flows and also for non-Newtonian fluids. There are three types of non-Newtonian fluids, such as differential, integral and rate types. Second grade fluid is a subclass of differential type fluids which exhibits the normal stress effects. To predict these effects many researchers studied second grade fluid under various aspects (see [2–6] and many refs. therein). Various investigations also examine the boundary layer flow of viscous and non-Newtonian fluids over a surface subject to linear and power law stretching velocities (see some recent studies [7–11]).

Much attention in the literature has been given to the flows by a linear stretching surface. However this seems not realistic when the processes for plastic and polymer extrusion are considered. In these processes stretching velocity is nonlinear. Very less attention is given to the flows generated by power law stretching velocities. Few investigations about the two-dimensional flows by an exponentially stretching surface have been presented. For example, thermal boundary layer by an exponentially stretching continuous surface in presence of applied magnetic field was investigated numerically by Al-Odat et al. [12]. Thermal radiation in flow of viscous fluid due to an exponentially stretching surface was studied by Sajid and Hayat [13]. Analytical solution of nanofluid flow over an exponential stretching surface was presented by Nadeem and

[1]The article is published in the original.

Lee [14]. Heat transfer analysis over an exponentially shrinking surface through the shooting method was investigated by Bhattacharyya [15]. Heat transfer effect in the flow of Casson fluid was studied by Mukhopadhyay et al. [16]. Mustafa et al. [17] presented the analysis of nanofluid flow over an exponentially stretching sheet in the presence of the convective boundary conditions. Recently, three-dimensional flow of viscous fluid over an exponentially stretching surface with heat transfer was studied by Liu et al. [18]. Many investigators also stressed on the magnetohydrodynamic flow of an electrically conducting fluid because of its numerous applications in metallurgical industry such as in drawing, annealing, in the purification of molten metals from non-metallic inclusions, electromagnetic pumps, MHD generators etc. Several studies have been presented by the authors for stretched flow in presence of transverse magnetic field. Magnetohydrodynamic boundary layer flow of viscous fluid with variable viscosity over a stretching surface was presented by Mukhopadhyay et al. [19]. Motsa et al. [20] addressed the flow of upper convected Maxwell fluid over porous stretching sheet in presence of magnetic field. The authors used the successive Taylor series linearization method. Rashidi and Erfani [21] studied the stagnation-point flow in presence of porous media and magnetic field.

There are several processes where forced and free convection act simultaneously to establish the flow regime, temperature and concentration fields around a heated/cooled permeable/impermeable plate or stretching sheet. Examples include flow in electronic equipment cooled by a fan, flows in the ocean and in the atmosphere, solar receivers exposed to wind currents, electronic devices cooled by fans, nuclear reactors cooled during emergency shutdown, heat exchangers placed in a low-velocity environment and many more. Unsteady mixed convective flow and heat transfer over a stretching surface in the presence of slip was determined by Mukhophadhyay [22]. Mixed convection flow of MHD stagnation point flow over a vertical stretching sheet with a thermal radiation was obtained by Hayat et al. [23]. Recently, Turkyilmazoglu [24] discussed the mixed convection flow over a permeable stretching surface. Heat source or sink in moving fluids assumes a greater significance in all situations which deal with exothermic or endothermic chemical reaction and concerned with dissociating fluids [25, 26]. More often investigators considered the surface temperature and heat flux situations for the stretching surface. Recently convective boundary is used for the heat transfer from the surface (see [27–29]). However, according to our knowledge no analysis has been given yet for the flow employing the convective condition of mass transfer over a stretching surface.

The purpose of present investigation is to deal with the three-dimensional flow of viscoelastic fluid by an exponentially stretching surface. Formulation is made in the presence of a heat source/sink. Heat and mass transfer effects in the presence of chemical reaction and mixed convection are also studied. A uniform magnetic field is applied along the normal to the flow direction. Convective boundary conditions for heat and mass transfer over the surface have been taken into account. Similarity transformations are used to reduce the partial differential equations into the ordinary differential equations. Convergent solutions are obtained by using the homotopy analysis method [30–40]. Impacts of all the physical parameters involved in the flow problems are analyzed for the flow field, temperature and concentration.

1. MATHEMATICAL MODELING

We consider the three-dimensional mixed convection boundary layer flow of viscoelastic fluid over an exponentially stretching surface in the presence of an internal heat source/sink and generative/destructive chemical reaction. Magnetic field is applied in the transverse direction of the flow. The surface coincides with the plane at $z = 0$ and the flow is confined in the region $z > 0$. Convective boundary conditions for both heat and mass transfer on the surface of a sheet are chosen. The governing boundary layer equations for three dimensional flow can be put into the forms:

$$\frac{\partial u}{\partial x} + \frac{\partial v}{\partial y} + \frac{\partial w}{\partial z} = 0,$$

$$u\frac{\partial u}{\partial x} + v\frac{\partial u}{\partial y} + w\frac{\partial u}{\partial z} = \nu\frac{\partial^2 u}{\partial z^2} + \frac{k_0}{\rho}$$
$$\times\left(u\frac{\partial^3 u}{\partial x\partial z^2} + w\frac{\partial^3 u}{\partial z^3} - \left(\frac{\partial u}{\partial x}\frac{\partial^2 u}{\partial z^2} + \frac{\partial u}{\partial z}\frac{\partial^2 w}{\partial z^2} + 2\frac{\partial u}{\partial z}\frac{\partial^2 u}{\partial x\partial z} + 2\frac{\partial w}{\partial z}\frac{\partial^2 u}{\partial z^2}\right)\right)$$
$$+ g\beta_T(T - T_\infty) + g\beta_C(C - C_\infty) - \frac{\sigma^* B_0^2}{\rho}u,$$

$$u\frac{\partial v}{\partial x}+v\frac{\partial v}{\partial y}+w\frac{\partial v}{\partial z}=v\frac{\partial^2 v}{\partial z^2}+\frac{k_0}{\rho}$$
$$\times\left(v\frac{\partial^3 v}{\partial y\partial z^2}+w\frac{\partial^3 v}{\partial z^3}-\left(\frac{\partial v}{\partial y}\frac{\partial^2 v}{\partial z^2}+\frac{\partial v}{\partial z}\frac{\partial^2 w}{\partial z^2}+2\frac{\partial v}{\partial z}\frac{\partial^2 v}{\partial y\partial z}+2\frac{\partial w}{\partial z}\frac{\partial^2 v}{\partial z^2}\right)\right)-\frac{\sigma^* B_0^2}{\rho}v,$$

$$u\frac{\partial T}{\partial x}+v\frac{\partial T}{\partial y}+w\frac{\partial T}{\partial z}=\sigma\frac{\partial^2 T}{\partial z^2}+\frac{Q}{\rho c_p}(T-T_\infty),$$

$$u\frac{\partial C}{\partial x}+v\frac{\partial C}{\partial y}+w\frac{\partial C}{\partial z}=D_B\frac{\partial^2 C}{\partial z^2}-k_1(C-C_\infty).$$

In the above equations, u, v, and w are the velocity components in the x-, y-, and z-directions, respectively, k_0 is the material fluid parameter, β_T is the thermal expansion coefficient, β_C is the concentration expansion coefficient, σ^* is the electrical conductivity, B_0 is the magnitude of applied magnetic field, ρ is the density of fluid, g is the gravitational acceleration, $\nu = (\mu / \rho)$ is the kinematic viscosity, μ is the dynamic viscosity, σ is the thermal diffusivity, T is the fluid temperature, c_p is the specific heat of the fluid, Q is the uniform volumetric heat generation/absorption, C is the concentration field, D is the mass diffusivity and prime denotes the differentiation with respect to η.

The boundary conditions can be expressed as follows:

$$u = U_w,\ v = V_w,\ w = 0,\ -k\frac{\partial T}{\partial z} = h(T_f - T),\ -D\frac{\partial T}{\partial z} = h^*(C_f - C) \text{ at } z = 0,$$
$$u \to 0,\ v \to 0,\ T \to T_\infty,\ C \to C_\infty \text{ as } z \to \infty,$$

where subscript w corresponds to the wall condition, h is the heat transfer coefficient, h^* is the concentration transfer coefficient, T_f is the ambient fluid temperature, and C_f is the ambient fluid concentration.

At wall the velocities, temperature and concentration distributions are defined as:

$$U_w = U_0 e^{\frac{x+y}{L}},\ V_w = V_0 e^{\frac{x+y}{L}},\ T_w = T_\infty + T_0 e^{\frac{A(x+y)}{2L}},\ C_w = C_\infty + C_0 e^{\frac{B(x+y)}{2L}},$$

where U_0, V_0, W_0 are the constants, L is the reference length, T_∞ is the ambient temperature, C_∞ is the ambient concentration, A is the temperature exponent, and B is the concentration exponent.

By using the transformations [18]:

$$u = U_0 e^{\frac{x+y}{L}} f'(\eta),\ v = U_0 e^{\frac{x+y}{L}} g'(\eta),\ w = -\left(\frac{vU_0}{2L}\right)^{1/2} e^{\frac{x+y}{2L}}(f + \eta f'' + g + \eta g'),$$
$$T = T_\infty + T_0 e^{\frac{A(x+y)}{2L}}\theta(\eta),\ C = C_\infty + C_0 e^{\frac{B(x+y)}{2L}}\varphi(\eta),\ \eta = \left(\frac{U_0}{2vL}\right)^{1/2} e^{\frac{x+y}{2L}} z$$

Eq. (1) is identically satisfied and Eqs. (2)–(9) give:

$$f''' + (f+g)f'' - 2(f'+g')f' + K$$
$$\times(6f'''f' + (3g'' - 3f'' + \eta g''')f'' + ((4g' + 2\eta g'')f''' - (f + g + \eta g')f'''')$$
$$+ 2\lambda(\theta + N\varphi) - 2Mf' = 0,$$

$$g''' + (f+g)g'' - 2(f'+g')g'$$
$$+ K(6g'''g' + (3f'' - 3g'' + \eta f''')g'' + (4f' + 2\eta f'')g''' - (f + g + \eta f')g'''') - 2Mg' = 0,$$

$$\theta'' + \Pr(f+g)\theta' - \Pr A(f'+g')\theta + \Pr\beta\theta = 0,$$

$$\varphi'' + \mathrm{Sc}(f+g)\varphi' - \mathrm{Sc}B(f'+g')\varphi - \mathrm{Sc}k\varphi = 0,$$

$$f = 0,\ g = 0,\ f' = 1,\ g' = \alpha,\ \theta' = -\gamma_1(1 - \theta(0)),\ \varphi' = -\gamma_2(1 - \varphi(0)),\ \text{at } \eta = 0,$$

$$f' \to 0,\ g' \to 0,\ \theta \to 0,\ \varphi \to 0 \text{ as } \eta \to \infty,$$

where K is the viscoelastic parameter, λ is the mixed convection parameter, Gr_x is the local Grashof number, N is the concentration buoyancy parameter, M is the Hartman number, Pr is the Prandtl number, β is the heat generation absorption parameter, k is the chemical reaction parameter, Sc is the Schmidt number, α is the ratio parameter, γ_1 is the heat transfer Biot number, and γ_2 is the mass transfer Biot number. These can be defined in the forms

$$K = \frac{k_0 U_w}{2\nu L},\ \lambda = \frac{\mathrm{Gr}_x}{\mathrm{Re}_x^2},\ \mathrm{Gr}_x = \frac{g\beta_T (T_f - T_\infty)x^3}{\nu^2},\ N = \frac{\beta_C (C_w - C_\infty)}{\beta_T (T_f - T_\infty)},\ \mathrm{M} = \frac{\sigma^* B_0^2}{\rho} e^{\frac{x+y}{L}},$$

$$\mathrm{Pr} = \frac{\nu}{\sigma},\ \beta = \frac{Q}{\rho c_p},\ k = \frac{k_1}{U_0},\ \mathrm{Sc} = \frac{\nu}{D},\ \alpha = \frac{V_0}{U_0},\ \gamma_1 = \frac{h}{k}\sqrt{\frac{\nu}{a}},\ \gamma_2 = \frac{h^*}{D}\sqrt{\frac{\nu}{a}}.$$

The local Nusselt and Sherwood numbers in dimensionless forms can be expressed as follows:

$$Nu/\mathrm{Re}_x^{1/2} = -\frac{x}{2L}\theta'(0),$$

$$Sh/\mathrm{Re}_x^{1/2} = -\frac{x}{2L}\varphi'(0),$$

in which $\mathrm{Re}_x = \frac{U_0 L}{\nu} e^{\frac{x+y}{L}}$ is the local Reynold number.

2. SERIES SOLUTIONS

For homotopic solutions, the initial guesses and auxiliary linear operators are chosen as

$$f_0(\eta) = \left(1 - e^{-\eta}\right),\ g_0(\eta) = \alpha\left(1 - e^{-\eta}\right),\ \theta_0(\eta) = \frac{\gamma_1 \exp(-\eta)}{1+\gamma_1},\ \varphi_0(\eta) = \frac{\gamma_2 \exp(-\eta)}{1+\gamma_2},$$

$$L_f = f''' - f',\ L_g = g''' - g',\ \ L_\theta = \theta'' - \theta,\ L_\varphi = \varphi'' - \varphi$$

with

$$L_f(C_1 + C_2 e^{\eta} + C_3 e^{-\eta}) = 0,\ L_g(C_4 + C_5 e^{\eta} + C_6 e^{-\eta}) = 0,$$

$$L_\theta(C_7 e^{\eta} + C_8 e^{-\eta}) = 0,\ L_\varphi(C_9 e^{\eta} + C_{10} e^{-\eta}) = 0,$$

where C_i $(i = 1-10)$ are the arbitrary constants.

Zeroth order deformation problems are

$$(1-p)L_f\left[\hat{f}(\eta;p) - f_0(\eta)\right] = p\hbar_f \mathbf{N}_f\left[\hat{f}(\eta;p), \hat{g}(\eta;p), \hat{\theta}(\eta;p), \hat{\varphi}(\eta;p)\right],$$

$$(1-p)L_g\left[\hat{g}(\eta;p) - g_0(\eta)\right] = p\hbar_g \mathbf{N}_g\left[\hat{f}(\eta;p), \hat{g}(\eta;p)\right],$$

$$(1-p)L_\theta\left[\hat{\theta}(\eta;p) - \theta_0(\eta)\right] = p\hbar_\theta \mathbf{N}_\theta\left[\hat{f}(\eta;p), \hat{g}(\eta;p), \hat{\theta}(\eta;p), \hat{\varphi}(\eta;p)\right],$$

$$(1-p)L_\varphi\left[\hat{\varphi}(\eta;p) - \varphi_0(\eta)\right] = p\hbar_\varphi \mathbf{N}_\varphi\left[\hat{f}(\eta;p), \hat{g}(\eta;p), \hat{\theta}(\eta;p), \hat{\varphi}(\eta;p)\right],$$

$$\hat{f}(0;p) = 0,\ \hat{f}'(0;p) = 1,\ \hat{f}'(\infty;p) = 0,\ \hat{g}(0;p) = 0, \hat{g}'(0;p) = \alpha, \hat{g}'(\infty;p) = 0,$$

$$\hat{\theta}'(0,p) = -\gamma_1[1 - \theta(0,p)],\ \hat{\theta}(\infty,p) = 0,\ \hat{\varphi}'(0,p) = -\gamma_2[1 - \hat{\varphi}(0,p)],\ \hat{\varphi}(\infty,p) = 0,$$

$$\mathbf{N}_f[\hat{f}(\eta;p), \hat{g}(\eta;p), \hat{\theta}(\eta;p), \hat{\varphi}(\eta;p)] = \frac{\partial^3 \hat{f}(\eta,p)}{\partial\eta^3} - 2\left(\frac{\partial \hat{f}(\eta,p)}{\partial\eta} + \frac{\partial \hat{g}(\eta,p)}{\partial\eta}\right)\frac{\partial \hat{f}(\eta,p)}{\partial\eta}$$

$$+ (\hat{f}(\eta,p) + \hat{g}(\eta,p))\frac{\partial^2 \hat{f}(\eta,p)}{\partial\eta^2} + 2\lambda(\hat{\theta}(\eta,p) + N\hat{\varphi}(\eta;p)) - 2\mathrm{M}\frac{\partial \hat{f}(\eta,p)}{\partial\eta}$$

$$+ K\left(6\frac{\partial \hat{f}(\eta,p)}{\partial\eta}\frac{\partial^3 \hat{f}(\eta,p)}{\partial\eta^3} + \left(3\frac{\partial^2 \hat{g}(\eta,p)}{\partial\eta^2} - 3\frac{\partial^2 \hat{f}(\eta,p)}{\partial\eta^2} + \eta\frac{\partial^3 \hat{g}(\eta,p)}{\partial\eta^3}\right)\frac{\partial^2 \hat{f}(\eta,p)}{\partial\eta^2}\right.$$

$$\left. + \left(4\frac{\partial \hat{g}(\eta,p)}{\partial\eta} + 2\eta\frac{\partial^2 \hat{g}(\eta,p)}{\partial\eta^2}\right)\frac{\partial^3 \hat{f}(\eta,p)}{\partial\eta^3} - \left(\hat{f}(\eta,p) + \hat{g}(\eta,p) + \eta\frac{\partial \hat{g}(\eta,p)}{\partial\eta}\right)\frac{\partial^4 \hat{f}(\eta,p)}{\partial\eta^4}\right),$$

$$\mathbf{N}_g[\hat{f}(\eta;p),\hat{g}(\eta;p),\hat{\theta}(\eta;p),\hat{\varphi}(\eta;p)] = \frac{\partial^3\hat{g}(\eta,p)}{\partial\eta^3} - 2\left(\frac{\partial\hat{f}(\eta,p)}{\partial\eta} + \frac{\partial\hat{g}(\eta,p)}{\partial\eta}\right)$$
$$\times\frac{\partial\hat{g}(\eta,p)}{\partial\eta} + \left(\hat{f}(\eta,p) + \hat{g}(\eta,p)\right)\frac{\partial^2\hat{g}(\eta,p)}{\partial\eta^2}$$
$$+ K\left(6\frac{\partial\hat{g}(\eta,p)}{\partial\eta}\frac{\partial^3\hat{g}(\eta,p)}{\partial\eta^3} + \left(3\frac{\partial^2\hat{f}(\eta,p)}{\partial\eta^2} - 3\frac{\partial^2\hat{g}(\eta,p)}{\partial\eta^2} + \eta\frac{\partial^3\hat{f}(\eta,p)}{\partial\eta^3}\right)\right)$$
$$+ K\left(\frac{\partial^2\hat{g}(\eta,p)}{\partial\eta^2} + \left(4\frac{\partial\hat{f}(\eta,p)}{\partial\eta} + 2\eta\frac{\partial^2\hat{f}(\eta,p)}{\partial\eta^2}\right)\frac{\partial^3\hat{g}(\eta,p)}{\partial\eta^3}\right)$$
$$- \left(\hat{f}(\eta,p) + \hat{g}(\eta,p) + \eta\frac{\partial\hat{f}(\eta,p)}{\partial\eta}\right)\frac{\partial^4\hat{g}(\eta,p)}{\partial\eta^4}\Bigg) - 2\mathrm{M}\frac{\partial\hat{g}(\eta,p)}{\partial\eta},$$

$$\mathbf{N}_\theta[\hat{f}(\eta;p),\hat{g}(\eta;p),\hat{\theta}(\eta;p),\hat{\varphi}(\eta;p)] = \frac{\partial^2\hat{\theta}(\eta,p)}{\partial\eta^2} + \mathrm{Pr}\left(\hat{f}(\eta,p) + \hat{g}(\eta,p)\right)\frac{\partial\hat{\theta}(\eta,p)}{\partial\eta}$$
$$-\mathrm{Pr}\,A\left(\frac{\partial\hat{f}(\eta,p)}{\partial\eta} + \frac{\partial\hat{g}(\eta,p)}{\partial\eta}\right)\hat{\theta}(\eta,p) + \mathrm{Pr}\,\beta\hat{\theta}(\eta,p),$$

$$\mathbf{N}_\varphi[\hat{f}(\eta;p),\hat{g}(\eta;p),\hat{\theta}(\eta;p),\hat{\varphi}(\eta;p)] = \frac{\partial^2\hat{\varphi}(\eta;p)}{\partial\eta^2} + \mathrm{Sc}\left(\hat{f}(\eta,p) + \hat{g}(\eta,p)\right)\frac{\partial\hat{\varphi}(\eta;p)}{\partial\eta}$$
$$-\mathrm{Sc}B\left(\frac{\partial\hat{f}(\eta,p)}{\partial\eta} + \frac{\partial\hat{g}(\eta,p)}{\partial\eta}\right)\hat{\varphi}(\eta;p) - \mathrm{Sc}k\hat{\varphi}(\eta;p).$$

Here p is an embedding parameter, the non-zero auxiliary parameters are $\hbar_f$, $\hbar_g$, $\hbar_\theta$, and $\hbar_\varphi$ and the non-linear operators are $\mathbf{N}_f$, $\mathbf{N}_g$, $\mathbf{N}_\theta$, and $\mathbf{N}_\varphi$. Taking $p = 0$ and 1 we get

$$\hat{f}(\eta;0) = f_0(\eta),\ \hat{g}(\eta;0) = g_0(\eta),\ \hat{\theta}(\eta,0) = \theta_0(\eta),\ \hat{\varphi}(\eta;0) = \varphi_0(\eta)\ \text{and}\ \hat{f}(\eta;1) = f(\eta),$$
$$\hat{g}(\eta;1) = g(\eta),\ \hat{\theta}(\eta,1) = \theta(\eta),\ \hat{\varphi}(\eta;1) = \varphi(\eta).$$

As p varies from 0 to 1 then $f(\eta,p)$, $g(\eta,p)$, $\theta(\eta,p)$, and $\varphi(\eta,p)$ differ from $f_0(\eta)$, $g_0(\eta)$, $\theta_0(\eta)$, and $\varphi_0(\eta)$ to $f(\eta)$, $g(\eta)$, $\theta(\eta)$, and $\varphi(\eta)$. Applying Taylors' expansion we attain

$$f(\eta,p) = f_0(\eta) + \sum_{m=1}^{\infty} f_m(\eta)p^m,\ f_m(\eta) = \frac{1}{m!}\frac{\partial^m f(\eta;p)}{\partial p^m}\bigg|_{p=0},$$

$$g(\eta,p) = g_0(\eta) + \sum_{m=1}^{\infty} g_m(\eta)p^m,\ g_m(\eta) = \frac{1}{m!}\frac{\partial^m g(\eta;p)}{\partial p^m}\bigg|_{p=0},$$

$$\theta(\eta,p) = \theta_0(\eta) + \sum_{m=1}^{\infty} \theta_m(\eta)p^m,\ \theta_m(\eta) = \frac{1}{m!}\frac{\partial^m \theta(\eta;p)}{\partial p^m}\bigg|_{p=0},$$

$$\varphi(\eta,p) = \varphi_0(\eta) + \sum_{m=1}^{\infty} \varphi_m(\eta)p^m,\ \varphi_m(\eta) = \frac{1}{m!}\frac{\partial^m \varphi(\eta;p)}{\partial p^m}\bigg|_{p=0}.$$

The convergence of the above series strongly depends upon $\hbar_f$, $\hbar_g$, $\hbar_\theta$, and $\hbar_\varphi$. Considering that $\hbar_f$, $\hbar_g$, $\hbar_\theta$, and $\hbar_\varphi$ are selected properly so that Eqs. (33)–(36) converge at $p = 1$. Therefore

$$f(\eta) = f_0(\eta) + \sum_{m=1}^{\infty} f_m(\eta),$$

Table 1. Convergence of series solutions for different order of approximations when $K = \mathrm{M} = 0.1$, $A = B = \beta = \alpha = 0.2$, $\lambda = N = k = 0.3$, $\gamma_1 = \gamma_2 = 0.5$, $\mathrm{Pr} = 0.7$, $\mathrm{Sc} = 0.8$, $\alpha = 0.2$, and $\hbar_f = \hbar_g = \hbar_\theta = \hbar_\varphi - 0.6$

Order of approximations	1	5	10	15	20	25	30	35
$-f''(0)$	1.155	1.104	1.078	1.068	1.065	1.064	1.064	1.064
$-g''(0)$	0.2359	0.2395	0.2414	0.2420	0.2422	0.2422	0.2422	0.2422
$-\theta'(0)$	0.3084	0.2620	0.2437	0.2373	0.2341	0.2341	0.2340	0.2340
$-\varphi'(0)$	0.3300	0.3318	0.3336	0.3340	0.3341	0.3341	0.3341	0.3341

$$g(\eta) = g_0(\eta) + \sum_{m=1}^{\infty} g_m(\eta),$$

$$\theta(\eta) = \theta_0(\eta) + \sum_{m=1}^{\infty} \theta_m(\eta),$$

$$\varphi(\eta) = \varphi_0(\eta) + \sum_{m=1}^{\infty} \varphi_m(\eta).$$

The general solution expressions can be written as

$$f_m(\eta) = f_m^*(\eta) + C_1 + C_2 e^{\eta} + C_3 e^{-\eta},$$

$$g_m(\eta) = g_m^*(\eta) + C_4 + C_5 e^{\eta} + C_6 e^{-\eta},$$

$$\theta_m(\eta) = \theta_m^*(\eta) + C_7 e^{\eta} + C_8 e^{-\eta},$$

$$\varphi_m(\eta) = \varphi_m^*(\eta) + C_9 e^{\eta} + C_{10} e^{-\eta},$$

where the special solutions are f_m^*, g_m^*, θ_m^*, and φ_m^*.

3. CONVERGENCE ANALYSIS AND DISCUSSION

The homotopic solutions (37)–(40) obviously depend on the auxiliary parameters $\hbar_f$, $\hbar_g$, $\hbar_\theta$, and $\hbar_\varphi$. In order to control the convergence of the series solutions these auxiliary parameters play a central role. To obtain the convergence region, the $\hbar$ is curves have been plotted at 14th order of approximations in Fig. 1. This figure clearly shows that the acceptable values of $\hbar_f$, $\hbar_g$, $\hbar_\theta$, and $\hbar_\varphi$ are $-1.0 \le \hbar_f \le -0.4$, $-1.0 \le \hbar_g \le -0.2$, $-1.2 \le \hbar_\theta \le -0.1$, and $-1.2 \le \hbar_\varphi \le -0.1$. Table 1 ensures that the series solutions converge in the whole region of η when $\hbar_f = \hbar_g = \hbar_\theta = \hbar_\varphi = -0.5$.

Figures 2–7 are plotted to see the effects of a viscoelastic parameter K, Hartman number M, ratio parameter α on the velocity profiles $f'(\eta)$ and $g'(\eta)$. Figures 2 and 3 display the variation of a viscoelastic parameter K on the velocity profiles $f'(\eta)$ and $g'(\eta)$. It is noticed that the velocity profiles and momentum boundary layer thicknesses increase with K. Effect of the Hartman number M on the velocity profiles $f'(\eta)$ and $g'(\eta)$ are plotted in the Figs. 4 and 5. The velocity profiles $f'(\eta)$ and $g'(\eta)$ are decreased when we increase the values of M. Also the momentum boundary layer thicknesses are decreasing functions of M. Figures 6 and 7 show the behavior of a ratio parameter α on the velocity profiles $f'(\eta)$ and $g'(\eta)$. It is found that the momentum boundary layer thickness and velocity profile $f'(\eta)$ decrease for larger values of α while the reverse behavior is examined for the velocity profile $g'(\eta)$. Figure 8 is drawn to see the influence of an internal heat source/ sink parameter β on the velocity profile $f'(\eta)$. Clearly in a case of the heat sink parameter $\beta < 0$ both the momentum boundary layer thickness and $f'(\eta)$ decrease while in a case of the heat source parameter $\beta > 0$ the kinetic energy of the fluid particles increases and thus the velocity profile $f'(\eta)$ increases. Outcome of a mixed convection parameter λ on the velocity profile $f'(\eta)$ in both an assisting and an opposing flows is seen in Fig. 9. In the case of an assisting flow $\lambda > 0$ both $f'(\eta)$ and momentum boundary layer thickness are enhanced while the reverse effect is observed for an opposing

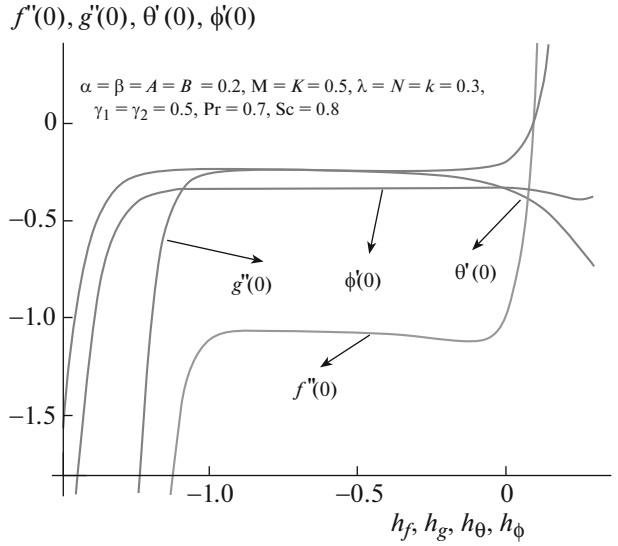

Fig. 1. $\hbar$ is curves for the function $f(\eta)$, $g(\eta)$, and $\theta(\eta)$.

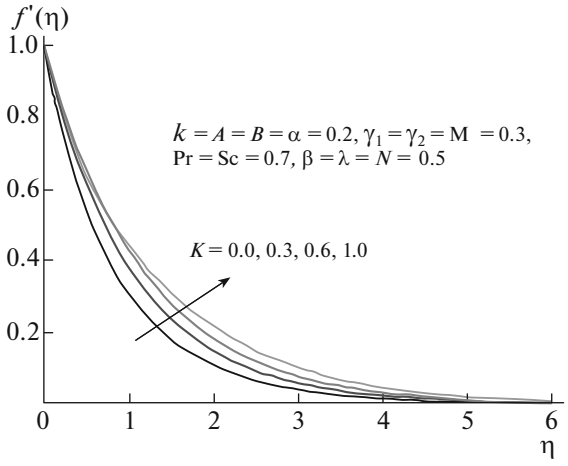

Fig. 2. Variation of K on $f'(\eta)$.

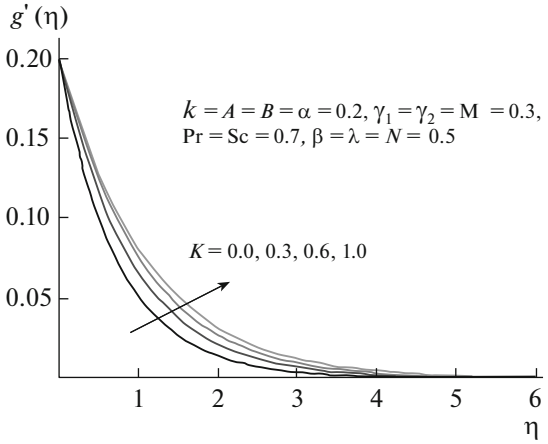

Fig. 3. Variation of K on $g'(\eta)$.

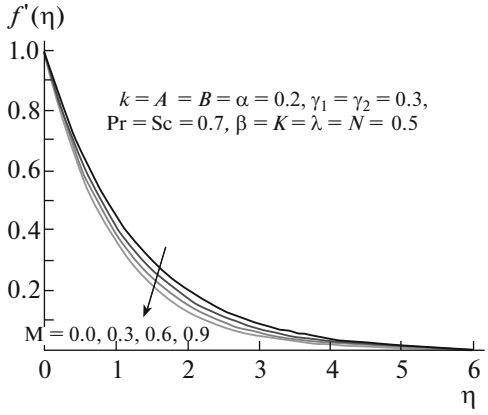

Fig. 4. Variation of M on $f'(\eta)$.

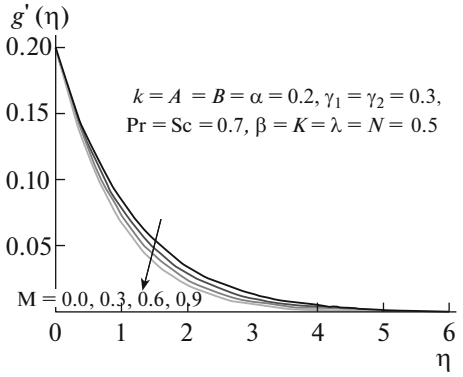

Fig. 5. Variation of M on $g'(\eta)$.

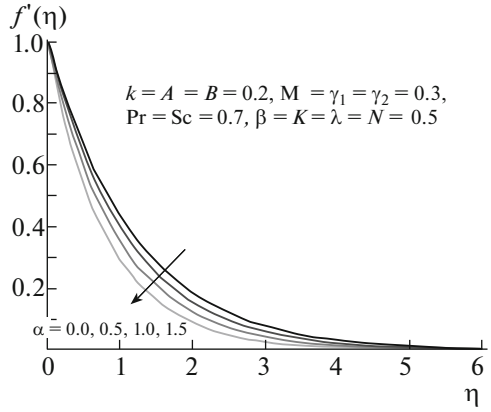

Fig. 6. Variation of α on $f'(\eta)$.

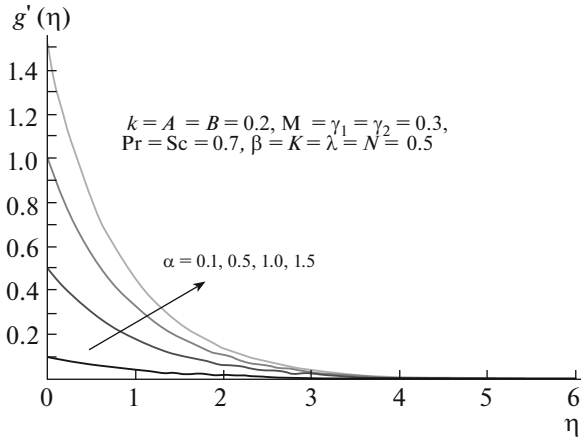

Fig. 7. Variation of α on $g'(\eta)$.

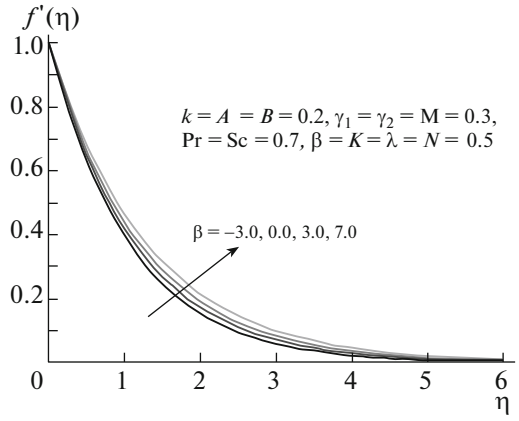

Fig. 8. Variation of β on $f'(\eta)$.

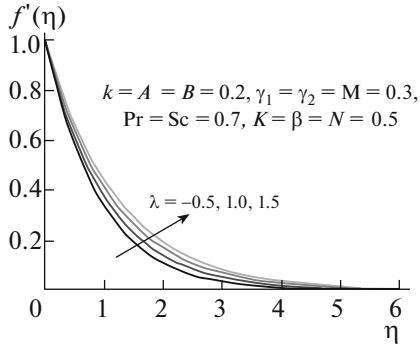

Fig. 9. Variation of λ on $f'(\eta)$.

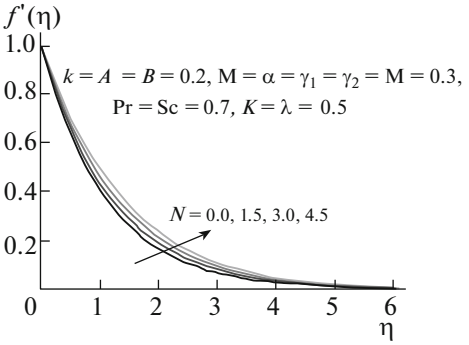

Fig. 10. Variation of N on $f'(\eta)$.

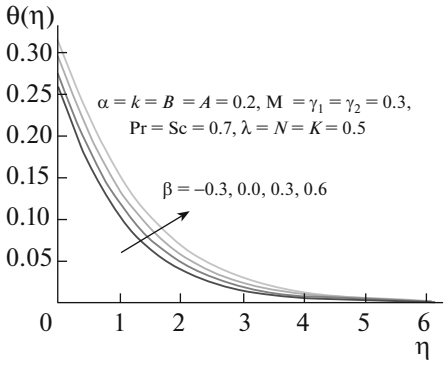

Fig. 11. Variation of β on θ(η).

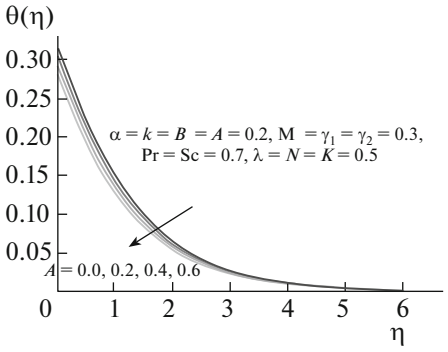

Fig. 12. Variation of A on θ(η).

flow $\lambda < 0$. Figure 10 exhibits the variation of the concentration buoyancy parameter N on the velocity profile $f'(\eta)$. It is examined that an enhancement in N gives rise to the velocity profile $f'(\eta)$.

Effects of an internal heat source/sink parameter β, temperature exponent A, heat transfer Biot number γ_1 and Prandtl number Pr on the temperature θ(η) are analyzed in the Figs. 11–14. Figure 11 depicts the influence of an internal heat source/sink parameter β on the temperature θ(η). With an increase in an internal heat source $\beta > 0$ both the thermal boundary layer thickness and θ(η) increase while in a case of the heat sink parameter $\beta < 0$ both the thermal boundary layer thickness and θ(η) decrease. Variation of the temperature exponent A on the temperature θ(η) is displayed in Fig. 12. It is found that with an

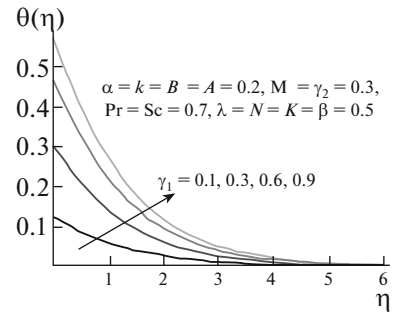

Fig. 13. Variation of γ_1 on $\theta(\eta)$.

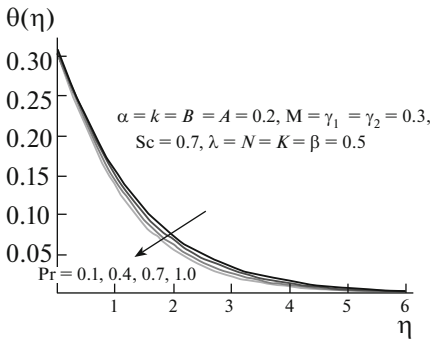

Fig. 14. Variation of Pr on $\theta(\eta)$.

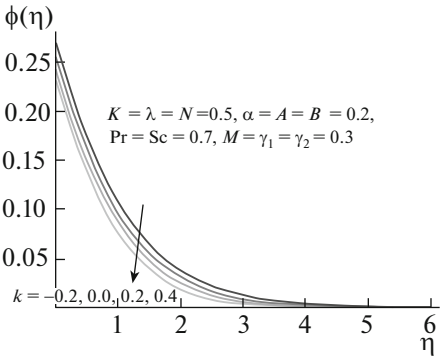

Fig. 15. Variation of k on $\phi(\eta)$.

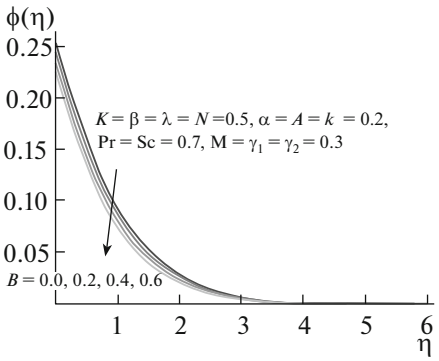

Fig. 16. Variation of B on $\phi(\eta)$.

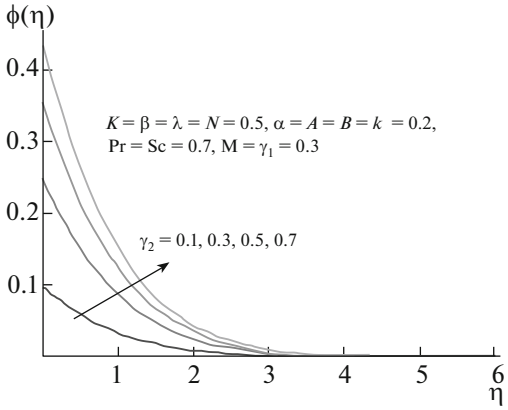

Fig. 17. Variation of γ_2 on $\phi(\eta)$.

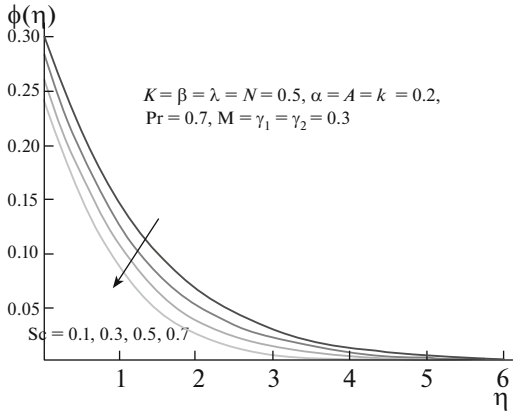

Fig. 18. Variation of Sc on $\phi(\eta)$.

increase in A the thermal boundary layer thickness as well as temperature $\theta(\eta)$ decreases. As the heat transfer Biot number γ_1 increases from zero, the temperature $\theta(\eta)$ boosts up (see Fig. 13). Also it is seen that the thermal boundary layer thickness is an increasing function of γ_1. Impact of the Prandtl number Pr on the temperature $\theta(\eta)$ is drawn in Fig. 14. As Prandtl number is the ratio of momentum to thermal diffusivities therefore an enhancement in Pr leads to decrease in the thermal diffusivity and consequently decrease in temperature $\theta(\eta)$ is noted.

Figures 15–18 are sketched to see the variations of a chemical reaction parameter k, concentration exponent B, mass transfer Biot number γ_2 and Schmidt number Sc on the concentration profile $\varphi(\eta)$. Figure 15 is displayed to analyze the variation of a chemical reaction parameter k on the concentration

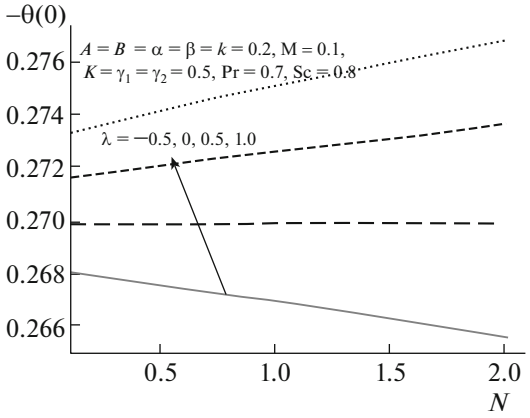

Fig. 19. Variations of λ and N on $-\theta'(0)$.

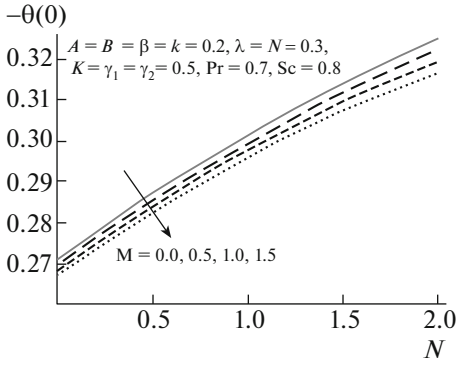

Fig. 20. Variations of M and α on $-\theta'(0)$.

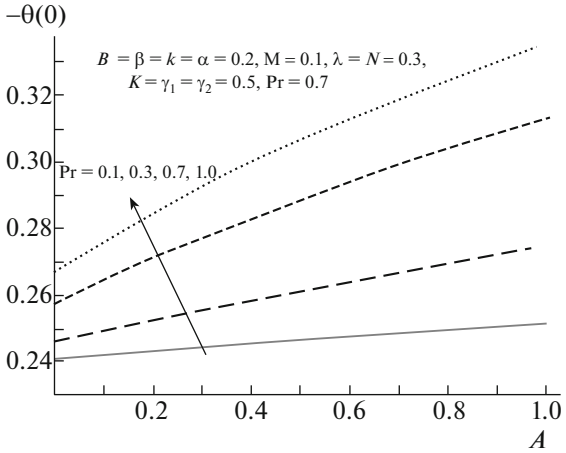

Fig. 21. Variations of A and Pr on $-\theta'(0)$.

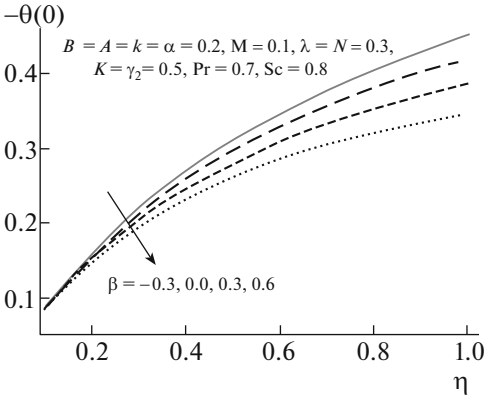

Fig. 22. Variations of β and γ_1 on $-\theta'(0)$.

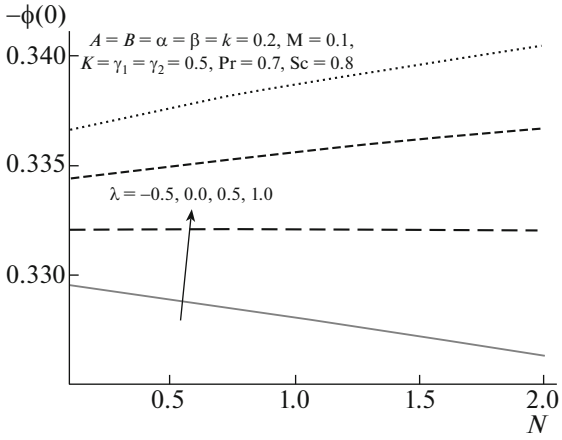

Fig. 23. Variations of λ and N on $-\phi'(0)$.

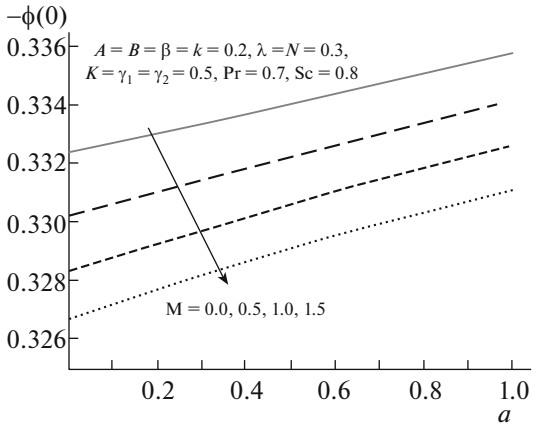

Fig. 24. Variations of M and α on $-\phi'(0)$.

profile $\varphi(\eta)$. It is noted that the associated boundary layer thickness and the concentration profile decrease for a generative chemical reaction when $k > 0$ while the reverse phenomenon is noted for a destructive chemical reaction for $k < 0$. With an enhancement in the concentration exponent B both the concentration profile $\varphi(\eta)$ and the boundary layer thickness decrease (see Fig. 16). Variation of the mass

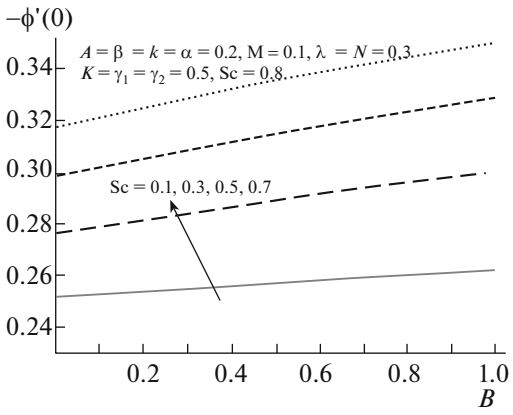

Fig. 25. Variations of Sc and B on $-\phi'(0)$.

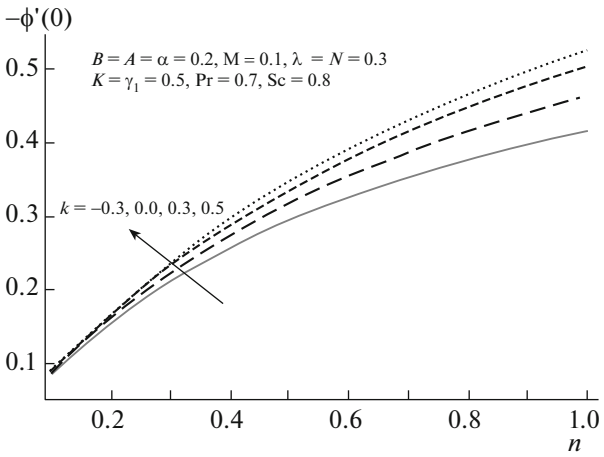

Fig. 26. Variations of k and γ_2 on $-\phi'(0)$.

transfer Biot number γ_2 on the concentration profile $\varphi(\eta)$ is displayed in Fig. 17. Here we examined that the effect of γ_2 on the concentration profile $\varphi(\eta)$ is similar to that of γ_1 on the temperature profile $\theta(\eta)$. Figure 18 is drawn to see the influence of the Schmidt number Sc on the concentration profile $\varphi(\eta)$. It is seen that with an enhancement in Sc the mass diffusivity decreases which shows a decrease in the concentration profile $\varphi(\eta)$.

Figures 19–22 are displayed to see the impacts of a mixed convection parameter λ, concentration buoyancy parameter N, ratio parameter α, Hartman number M, Prandtl number Pr, temperature exponent A, internal heat source/sink β and heat transfer Biot number γ_1 on the local Nusselt number $-\theta'(0)$. Figure 19 shows that the heat transfer rate at the wall increases for an assisting flow $\lambda > 0$ while it decreases for an opposing flow $\lambda < 0$. It is also examined that the heat transfer rate at the wall is increasing function of the concentration buoyancy parameter N. Figure 20 showed that the larger values of a ratio parameter α corresponds to a higher heat transfer rate $-\theta'(0)$. Also it is noted that with an increase in Hartman number the heat transfer rate decreases. Similar behaviors of the temperature exponent A and Prandtl number Pr are observed on the heat transfer rate at the wall $-\theta'(0)$ (see Fig. 21). Figure 22 depicts that the heat transfer rate at the wall $-\theta'(0)$ decreases with an internal heat generation $\beta > 0$ while it increases with an internal heat absorption $\beta < 0$.

Variations of a mixed convection parameter λ, concentration buoyancy parameter N, ratio parameter α, Hartman number M, Schmidt number Sc, concentration exponent B, chemical reaction k and mass transfer Biot number γ_2 on Sherwood number $-\varphi'(0)$ are plotted in the Figs. 23–26. Figure 23 is drawn to see the influences of a mixed convection parameter λ and concentration buoyancy parameter N on the Sherwood number $-\varphi'(0)$. It is seen that the Sherwood number $-\varphi'(0)$ is an increasing function of λ and N in the case of an assisting flow $\lambda > 0$ while a decreasing function for an opposing flow case. Figure 24 depicts that the Sherwood number $-\varphi'(0)$ decreases with an enhancement in Hartman number M while it

Table 2. Comparative values of $-f''(0)$, $-g''(0)$, and $f(\infty) + g(\infty)$ for different values of α when $K = \lambda = N = \gamma_1 = \gamma_2 = \beta = k = 0$

Liu et al. [18]			Present results			
α	$-f''(0)$	$-g''(0)$	$f(\infty) + g(\infty)$	$-f''(0)$	$-g''(0)$	$f(\infty) + g(\infty)$
0.0	1.28180856	0	0.90564383	1.28181	0	0.90564
0.50	1.56988846	0.78494423	1.10918263	1.56989	0.78494	1.10918
1.00	1.81275105	1.81275105	1.28077378	1.81275	1.81275	1.28077

increases with an increase in a ratio parameter α. The Sherwood number $-\varphi'(0)$ increases with an increase in the Schmidt number Sc and concentration exponent B (see Fig. 25). Figure 26 explains that the mass transfer at the wall $-\varphi'(0)$ enhances with a generative chemical reaction when $k > 0$ while it reduces with a destructive chemical reaction for $k < 0$. It is also observed that the mass transfer at the wall $-\varphi'(0)$ is an increasing function of the mass transfer Biot number γ_2. Table 2 ensures the validity of the present results with the Liu et al. [18] in a limiting sense.

CONCLUSIONS

The present study deals with the three-dimensional mixed convection flow of MHD viscoelastic fluid by an exponentially stretching surface in the presence of a heat source/sink and generative/destructive chemical reaction. The main outcomes of the present study are as follows.

Variation of a viscoelastic parameter K on the velocity profiles $f'(\eta)$ and $g'(\eta)$ is qualitatively opposite to that of Hartman number M.

Both the velocity profile $f'(\eta)$ and momentum boundary layer thickness are increasing functions of an internal heat source parameter $\beta > 0$, an assisting flow case $\lambda > 0$ and the concentration buoyancy parameter N. These quantities are decreasing functions of an internal heat sink parameter $\beta < 0$ and an opposing flow case $\lambda < 0$.

Thermal boundary layer thickness and temperature $\theta(\eta)$ decreases with an increase in an internal heat source $\beta < 0$, temperature exponent A and Prandtl number Pr while the thermal boundary layer thickness and temperature $\theta(\eta)$ increase when an internal heat source $\beta > 0$ and the heat transfer Biot number γ_1 are increased.

With an enhancement in a generative chemical reaction for $k > 0$, the concentration exponent B and the Schmidt number Sc the concentration profile $\varphi(\eta)$ decreases while concentration boundary layer thickness increases for larger mass transfer Biot number γ_2 and destructive chemical reaction when $k < 0$.

The heat transfer rate $-\theta'(0)$ boosts up in the case of an assisting flow $\lambda > 0$, the concentration buoyancy parameter N, a ratio parameter α, the heat transfer Biot number γ_1 and an internal heat sink parameter $\beta < 0$ while the heat transfer rate $-\theta'(0)$ reduces with an opposing flow $\lambda < 0$, the Hartman number M and an internal heat source $\beta > 0$.

With an increase in an assisting flow $\lambda > 0$, the concentration buoyancy parameter N, a ratio parameter α, the mass transfer Biot number γ_2 and a generative chemical reaction parameter for $k > 0$ the Sherwood number $-\varphi'(0)$ enhances while the reverse behavior is noted in case of an opposing flow $\lambda < 0$, the Hartman number M and a destructive chemical reaction parameter for $k < 0$.

ACKNOWLEDGMENTS

We are grateful for financial support for second author through scholarship from Higher Education Commission. Further useful suggestions of a reviewer are highly appreciated.

REFERENCES

1. L. J. Crane, "Flow past a stretching plate," Z. Angew. Math. Phys. **21**, 645–647 (1970).
2. M. M. Rashidi, A. J. Chamkha, and M. Keimanesh, "Application of multi-step differential transform method on flow of a second-grade fluid over a stretching or shrinking sheet," Am. J. Comput. Math. **6**, 119–128 (2011).
3. A. Ahmad and S. Asghar, "Flow of a second grade fluid over a sheet stretching with arbitrary velocities subject to a transverse magnetic field," Appl. Math. Lett. **24**, 1905–1909 (2011).
4. T. Hayat, S. A. Shehzad, M. Qasim, and S. Obaidat, "Flow of a second grade fluid with convective boundary conditions," Thermal Sci. S **15**, 253–261 (2011).
5. M. Nazar, C. Fetecau, D. Vieru, and C. Fetecau, "New exact solutions corresponding to the second problem of Stokes for second grade fluids," Nonlinear Anal. Real World Appl. **11**, 584–591 (2010).

6. R. Nazar and N. A. Latip, "Numerical investigation of three-dimensional boundary layer flow due to a stretching surface in a viscoelastic fluid," Eur. J. Sci. Res. **29**, 509–517 (2009).
7. K. Bhattacharyya, M. S. Uddin, G. C. Layek, and M. A. Malek, "Effect of chemically reactive solute diffusion on boundary layer flow past a stretching surface with suction or blowing," J. Math. Math. Sci. **25**, 41–48 (2010).
8. R. Cortell, "Viscous flow and heat transfer over a nonlinearly stretching sheet," Appl. Math. Comput. **184**, 864–873 (2007).
9. S. Abbasbandy, H. R. Ghehsareh, and I. Hashim, "An approximate solution of the MHD flow over a nonlinearly stretching sheet by rational Chebyshev collocation method," UPB. Sci. Bull. **74** (2012).
10. S. Mukhopadhyay, "Casson fluid flow and heat transfer over a nonlinearly stretching surface," Chin. Phys. B **22**, 074701 (2013).
11. M. Turkyilmazoglu and I. Pop, "Exact analytical solutions for the flow and heat transfer near the stagnation point on a stretching/shrinking sheet in a Jeffrey fluid," Int. J. Heat Mass Transf. **57**, 82–88 (2013).
12. M. Q. Al-Odat, R. A. Damesh, and T. A. Al-Azab, "Thermal boundary layer on an exponentially stretching continuous surface in the presence of magnetic field," Int. J. Appl. Mech. Eng. **11**, 289–299 (2006).
13. M. Sajid and T. Hayat, "Influence of thermal radiation on the boundary layer flow due to an exponentially stretching sheet," Int. Commun. Heat Mass Transfer **35**, 347–356 (2008).
14. S. Nadeem and C. Lee, "Boundary layer flow of nanofluid over an exponentially stretching surface," Nanoscale Res. Lett. **7**, 94 (2012).
15. K. Bhattacharyya, "Boundary layer flow and heat transfer over an exponentially shrinking sheet," Chin. Phys. Lett. **28**, 074701 (2011).
16. S. Mukhopadhyay, K. Vajravelu, and R. A. V. Gorder, "Casson fluid flow and heat transfer at an exponentially stretching permeable surface," J. Appl. Mech. **80**, 054502 (2013).
17. M. Mustafa, T. Hayat, and S. Obaidat, "Boundary layer flow of a nanofluid over an exponentially stretching sheet with convective boundary conditions," Int. J. Numer. Meth. Heat Fluid Flow **23**, 945–959 (2013).
18. I. C. Liu, H. H. Wang, and Y. F. Peng, "Flow and heat transfer for three dimensional flow over an exponentially stretching surface," Chem. Eng. Commun. **200**, 253–268 (2013).
19. S. Mukhopadhyay, G. C. Layek, and S. K. A. Samad, "Study of MHD boundary layer flow over a heated stretching sheet with variable viscosity," Int. J. Heat Mass Transf. **48**, 4460–4466 (2005).
20. S. S. Motsa, T. Hayat, and O. M. Aldossary, "MHD flow of upper-convected Maxwell fluid over porous stretching sheet using successive Taylor series linearization method," Appl. Math. Mech. **33**, 975–990 (2012).
21. M. M. Rashidi and E. Erfani, "A new analytical study of MHD stagnation-point flow in porous media with heat transfer," Comput. Fluids **40**, 172–178 (2011).
22. S. Mukhopadhyay, "Effects of slip on unsteady mixed convective flow and heat transfer past a stretching surface," Chin. Phys. Lett. **27**, 124401 (2010).
23. T. Hayat, Z. Abbas, I. Pop, and S. Asghar, "Effects of radiation and magnetic field on the mixed convection stagnation-point flow over a vertical stretching sheet in a porous medium," Int. J. Heat Mass Transf. **53**, 466–474 (2010).
24. M. Turkyilmazoglu, "The analytical solution of mixed convection heat transfer and fluid flow of a MHD viscoelastic fluid over a permeable stretching surface," Int. J. Mech. Sci. **77**, 263–268 (2013).
25. E. M. A. Elbashbeshy and D. A. Aldawody, "Heat transfer over an unsteady stretching surface with variable heat flux in the presence of a heat source or sink," Comput. Math. Appl. **60**, 2806–2811 (2010).
26. R. Kandasamy, T. Hayat, and S. Obaidat, "Group theory transformation for Soret and Dufour effects on free convective heat and mass transfer with thermophoresis and chemical reaction over a porous stretching surface in the presence of heat source/sink," Nuclear Eng. Design **241**, 2155–2161 (2011).
27. A. Aziz, "A similarity solution for laminar thermal boundary layer over a flat plate with a convective surface boundary condition," Commun. Nonlinear Sci. Numer. Simul. **14**, 1064–1068 (2009).
28. O. D. Makinde and A. Aziz, "Boundary layer flow of a nanofluid past a stretching sheet with a convective boundary condition," Int. J. Therm. Sci. **50**, 1326–1332 (2011).
29. S. A. Shehzad, T. Hayat, and A. Alsaedi, "Three-dimensional flow of Jeffery fluid with convective surface boundary conditions," Int. J. Heat Mass Transf. **55**, 3971–3976 (2012).
30. M. M. Rashidi, N. F. Mehr, A. Hosseini, O. A. Bég, and T. K. Hung, "Homotopy simulation of nanofluid dynamics from a nonlinearly stretching isothermal permeable sheet with transpiration," Meccanica. doi 10.1007/s11012-013-9805-9
31. Y.P. Liu, S. J. Liao, and Z. B. Li, "Symbolic computation of strongly nonlinear periodic oscillations," J. Symb. Comput. **55**, 72–95 (2013).

32. S. Abbasbandy, M. S. Hashemi, and I. Hashim, "On convergence of homotopy analysis method and its application to fractional integro-differential equations," Quaestiones Math. **36**, 93–105 (2013).

33. L. Zheng, J. Niu, X. Zhang, and Y. Gao, "MHD flow and heat transfer over a porous shrinking surface with velocity slip and temperature jump," Math. Comput. Model. **56**, 133–144 (2012).

34. M. M. Rashidi, S.C. Rajvanshi, and M. Keimanesh, "Study of Pulsatile flow in a porous annulus with the homotopy analysis method," Int. J. Numer. Methods Heat Fluid Flow **22**, 971–989 (2012).

35. M. Turkyilmazoglu, "Solution of Thomas–Fermi equation with a convergent approach," Commun. Nonlinear Sci. Numer. Simul. **17**, 4097–4103 (2012).

36. T. Hayat, M. B. Ashraf, H. H. Alsulami, and M. S. Alhuthali, "Three dimensional mixed convection flow of viscoelastic fluid with thermal radiation and convective conditions," Plos One **9**, e90038 (2014).

37. H. N. Hassan and M. M. Rashidi, "An analytic solution of micropolar flow in a porous channel with mass injection using homotopy analysis method," Int. J. Numer. Methods Heat Fluid Flow **24** (2), 419–437 (2014).

38. T. Hayat, S. A. Shehzad, M. B. Ashraf, and A. Alsaedi, "Magnetohydrodynamic mixed convection flow of thixotropic fluid with thermophoresis and Joule heating," J. Thermophys. Heat Transf. **27**, 733–740 (2013).

39. T. Hayat, M. B. Ashraf, and A. Alsaedi, "Small-time solutions for the thin-film flow of a Casson fluid due to a suddenly moved plate," J. Aerosp. Eng. **27**, 04014034 (2014).

40. T. Hayat, M. Farooq, and A. Alsaedi, "Melting heat transfer in the stagnation point flow of Maxwell fluid with double-diffusive convection," Int. J. Numer. Methods Heat Fluid Flow **24**, 760–774 (2014).